ELSEVIER

Catalysis Today 39 (1998) 317–328

CATALYSIS TODAY

Nucleation and growth of Pd clusters in mordenite

Scott N. Reifsnyder, Mark M. Otten, H. Henry Lamb*

Department of Chemical Engineering, North Carolina State University, Box 7905, Raleigh, NC 27695, USA

Abstract

The nucleation and growth of Pd clusters in mordenite were investigated using in situ extended X-ray absorption fine structure (EXAFS) spectroscopy and Fourier transform infrared (FTIR) spectroscopy of adsorbed CO. Calcination of $[Pd(NH_3)_4]^{2+}$-exchanged mordenite at 350°C in O_2 results in decomposition of the amine complex and formation of square-planar Pd^{2+} oxo species within the mordenite pores. Reduction of these species at 150°C in H_2 yields Pd clusters with an average nuclearity of 3. On an average two 2.22 Å Pd–O bonds are associated with each Pd_3 cluster; we infer that this interaction serves to anchor the clusters within the pores. After reduction at 150°C, the FTIR spectrum of irreversibly adsorbed CO is indicative of a mixture of Pd^{+}, $Pd^{\delta+}$, and Pd^{0} carbonyl species. Reduction at 350°C produces larger intrazeolitic Pd clusters (average nuclearity of 6) that exhibit only a weak interaction with the mordenite, as evidenced by their facile aggregation in the presence of CO at 30°C. Reduction at 450°C yields large 20 Å Pd clusters that we infer are located on external mordenite surfaces or locally disrupt the intracrystalline structure. © 1998 Elsevier Science B.V.

Keywords: Palladium catalysts; Metal clusters; Mordenite; Metal-support interaction; EXAFS spectroscopy

1. Introduction

Our interest in zeolites as supports for transition metal complexes and clusters is motivated by the opportunities to create unique catalytic sites within well-ordered intracrystalline environments. Zeolites can stabilize small metal clusters with novel catalytic properties arising from intrinsic size effects and specific chemical interactions with the microporous support. Small electron-deficient $Pd^{\delta+}$ clusters in hydrogen zeolites have been investigated extensively by Sachtler and Zhang [1]. The concepts of ''proton anchoring'' and ''metal-proton adduct'' were introduced to explain the stabilization of small Pd clusters in acidic zeolites and the high catalytic activity of these entities for hydrocarbon conversion.

Mordenite has a unidirectional pore structure consisting of parallel, non-intersecting 6.7×7.0 Å elliptical channels. Dealuminated mordenite contains mesopores and may incorporate non-framework Al species that engender Lewis acidity [2]. Carvill et al. [3] investigated the effects of Pd^{2+} aquo complex formation in the precursor on the structure and performance of Pd-mordenite catalysts. Shpiro et al. [4] characterized small Pd clusters in mordenite by X-ray photoelectron spectroscopy (XPS) and electron paramagnetic resonance (EPR). An EPR signal was observed that is consistent with ''small Pd clusters carrying a partial positive charge''.

In this work, the nucleation and growth of Pd clusters in mordenite were investigated using in situ

*Corresponding author. Tel.: +1 919 515 6395; fax: +1 919 515 3465; e-mail: lamb@che.ncsu.edu

PII S0920-5861(97)00121-1

extended X-ray absorption fine structure (EXAFS) spectroscopy and Fourier transform infrared (FTIR) spectroscopy of adsorbed CO. EXAFS spectroscopy is an extremely valuable technique for characterizing supported metal clusters [5]. Complementary information on Pd oxidation state and dispersion is provided by FTIR spectroscopy of adsorbed CO [6].

2. Experimental methods

2.1. Catalyst preparation

Na-mordenite (Na-MOR) (5 g, Tosoh, SiO_2/Al_2O_3=18.5) was exchanged three times with a 2 M NH_4NO_3 solution to form NH_4-mordenite (NH_4-MOR). A 2500 ppm solution of $[Pd(NH_3)_4][NO_3]_2$ in deionized (DI) water was added dropwise to a slurry of NH_4-MOR (4 g) in DI water (50 ml). After 24 h, the solid was recovered by filtration, washed with DI water, and dried in air at 100°C. The $[Pd(NH_3)_4]^{2+}$-exchanged mordenite was calcined by heating at 0.5°C/min to 350°C in flowing O_2 (600 ml/min, extra dry); the final calcination temperature was maintained for 2 h. Upon cooling in O_2 the catalyst powder was light pink; subsequent exposure to air resulted in a change to light yellow. The resultant 0.5 wt% Pd-mordenite catalyst (Pd-MOR) was stored in a desiccator.

2.2. Temperature-programmed reduction (TPR)

Catalyst samples (0.4 g) were dried in flowing He (100 ml/min) for 1 h at 200°C and cooled to <30°C. The gas stream was switched to 5% H_2/Ar, and the reactor purged until a constant baseline was observed on a thermal conductivity detector (TCD). The sample was then heated (10°C/min) to 550°C, and the thermal conductivity difference between the H_2/Ar gas entering and exiting the TPR reactor was recorded. A coil of tubing located between the reactor exit and the TCD was immersed in an acetone/liquid N_2 slush bath to trap condensible gases.

2.3. EXAFS spectroscopy

X-ray absorption measurements were made on beamline X-11A of the National Synchrotron Light Source at Brookhaven National Laboratory. The storage-ring energy was 2.5 GeV and the current decayed from 250 to 110 mA during a typical fill. The beamline monochromator was equipped with a pair of Si(3 1 1) crystals for operation in the region of the Pd K edge (24 350 eV). Transmission X-ray absorption spectroscopy (XAS) data were recorded using an Ar-filled ionization chamber to measure the incident beam intensity (I_0) and a Kr-filled ionization chamber to measure the transmitted beam intensity (I).

The catalyst treatment station has been described previously [7]. XAS measurements were made with samples cooled to approximately −170°C. The Pd-MOR catalyst was heated in vacuo at 200°C for 0.5 h and cooled to <30°C, and the cell was backfilled with He prior to XAS. Subsequently, Pd-MOR catalysts were treated in flowing H_2 at the reduction temperature for 1.0 h. After cooling, XAS spectra were recorded with the samples under H_2. Samples were subsequently evacuated at 150°C or 300°C using a turbomolecular pump; the cell was backfilled with He at 30°C prior to XAS. Following H_2 treatment at 350°C and subsequent evacuation at 300°C, a Pd-MOR catalyst was exposed to 100 Torr CO at 30°C. The cell was evacuated and backfilled at 30°C prior to XAS.

Normalized EXAFS spectra were isolated from the experimental data using standard procedures [7], and the resultant spectra were fit in r space [8]. The Pd–Pd reference was derived from the EXAFS spectrum of Pd foil measured at −196°C. The Pd–O contributions were fit using a reference derived from the EXAFS spectrum of Rh_2O_3 (N=6, R=2.05 Å). The Pd–Si reference was calculated using the FEFF3 code (N=6, R=3.40 Å) [9].

2.4. FTIR spectroscopy

Infrared spectra were measured using an Analect RFX-65 FTIR spectrometer equipped with a high-sensitivity mercury–cadmium–telluride (MCT) detector. The in situ FTIR cell and treatment manifold have been described previously [10].

Catalyst samples were dried in vacuo at 150°C for 1 h. After cooling to <50°C, the catalysts were treated in flowing H_2 at the reduction temperature for 1 h and cooled to <50°C. The cell was subsequently evacuated and the catalyst heated at the evacuation temperature

for 1 h. Upon cooling to <30°C, the sample was exposed to 100 Torr of CO at 30°C for 15 min before recording the FTIR spectrum of reversibly adsorbed CO. Following evacuation to 10^{-6} Torr, the FTIR spectrum of irreversibly adsorbed CO was recorded. Difference spectra were obtained by subtraction of the catalyst spectrum immediately before CO exposure and normalized to the zeolite framework absorption at 2000 cm^{-1}. The spectra of reversibly adsorbed CO were corrected by subtracting the spectrum of gas-phase CO at 100 Torr.

3. Results

3.1. TPR

The TPR spectrum of Pd-MOR is shown in Fig. 1. The peak at 100°C is attributed to reduction of Pd^{2+} to Pd^0, as the peak area corresponds to consumption of 1.9 H/Pd. The high-temperature peaks are ascribed to hydrogen consumption due to reduction of impurities (e.g., Fe^{2+}).

3.2. EXAFS spectroscopy

The Pd K edge EXAFS spectrum of Pd-MOR after storage in air and subsequent evacuation at 200°C in an in situ XAS cell is shown in Fig. 2(a). The monotonically decreasing amplitude and low-frequency of the EXAFS oscillations indicate the presence of only low-Z backscatterers. The Pd–O phase-corrected Fourier transform (3.8<k<13.5 $Å^{-1}$) (Fig. 2(b)) contains a prominent peak near 2 Å and a smaller peak near 3.5 Å. The spectrum was fit in r space (1.0<r<3.5 Å, Pd–O phase correction) using Pd–O and Pd–Si contributions. The results (Table 1) evidence that the Pd is coordinated by ca. 4 oxygens at 2.03 Å; this shell is well ordered, as indicated by the low Debye–Waller factor. The Pd–Si distance (3.32 Å) is consistent with second nearest-neighbor (NN) Si or Al atoms in the zeolite framework. Comparisons of the experimental and calculated EXAFS functions in k and r space are shown in Fig. 2.

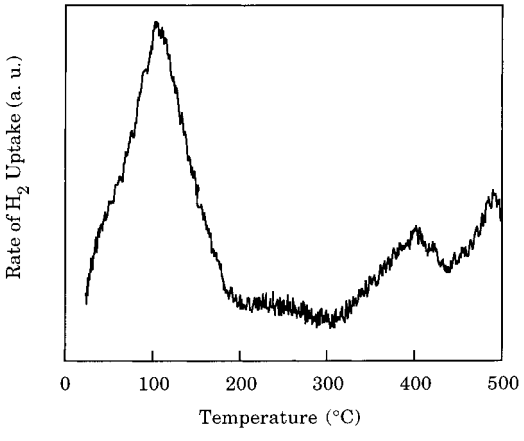

Fig. 1. TPR spectrum of Pd-MOR.

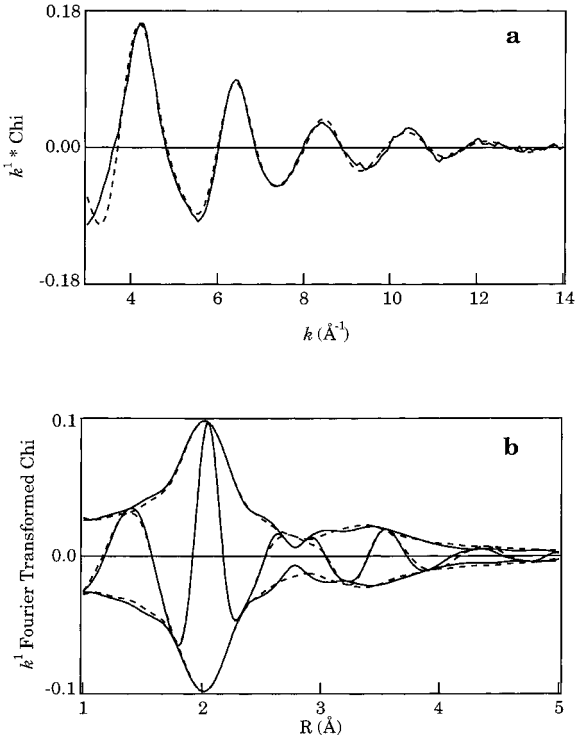

Fig. 2. Comparisons of Pd K first-shell EXAFS data (solid line) and calculated fit (dashed line) in k and r space for Pd-MOR: (a) k^1-weighted chi functions and (b) k^1-weighted Rh_2O_3 phase-corrected Fourier transforms.

The EXAFS spectrum of Pd-MOR after reduction at 150°C in flowing H_2 {Pd-MOR(150)} is shown in Fig. 3(a). False-EXAFS oscillations tentatively associated with beam instability limit the useful data range to k<11 $Å^{-1}$. Relative to the spectrum of the catalyst prior to reduction (Fig. 2(a)), the EXAFS oscillations

Table 1
Pd K edge EXAFS results for 0.5 wt% Pd-MOR catalysts

Treatment	Pd–Pd shell				Pd–O shell				Pd–Si shell			
	N^a	R^b	$\Delta\sigma^{2\,c}$	$\Delta E_0{}^d$	N^a	R^b	$\Delta\sigma^{2\,c}$	$\Delta E_0{}^d$	N^a	R^b	$\Delta\sigma^{2\,c}$	$\Delta E_0{}^d$
350°C, O_2 (ex situ)[e]					3.6	2.03	0.0001	−0.7	3.3	3.32	0.0094	0.6
150°C, H_2	2.1	2.77	0.0069	2.2	0.6	2.22	0.0000	0.9				
150°C, H_2; 150°C, vac	3.1	2.77	0.0066	−1.0	0.6	2.21	0.0030	0.0				
150°C, H_2; 300°C, vac	4.2	2.67	0.0138	3.3	0.8	1.97	0.0054	0.0				
350°C, H_2	4.2	2.78	0.0067	2.4								
350°C, H_2; 300°C, vac	5.5	2.71	0.0087	0.4								
350°C, H_2; 300°C, vac 30°C, CO	7.7	2.76	0.0037	5.3								
450°C, H_2	8.0	2.81	0.0052	−1.0								

[a]Coordination number (±15%).
[b]NN distance (±0.01 Å).
[c]Relative Debye–Waller factor (Å^2).
[d]Inner potential correction (eV).
[e]Treatment followed by in situ evacuation at 200°C.

have increased in frequency, and the low-k amplitude has decreased. These changes are consistent with Pd^{2+} reduction to Pd^0 with subsequent aggregation to form small clusters. The Pd–Pd phase-corrected Fourier transform ($2.8<k<10.9$ Å^{-1}) in Fig. 3(b) exhibits a first-shell peak due to Pd NN but no higher-shell peaks. A low-r sidelobe is observed which is indicative of a Pd low-Z contribution. The EXAFS spectrum was fit in r space ($1.0<r<3.5$ Å, uncorrected), and comparisons of the experimental and calculated EXAFS functions are shown in Fig. 3. The results (Table 1) indicate that the Pd clusters have a nuclearity of ca. 3 and a Pd NN distance slightly greater than in bulk Pd (2.75 Å). A Pd–O contribution was introduced in order to fit the low-r sidelobe on the main Pd–Pd peak. The fitting results (Table 1) indicate the presence of oxygen backscatterers at 2.22 Å; the Pd–O Debye–Waller factor is low and equivalent to that found for the Pd–O shell in the calcined catalyst.

The EXAFS spectrum of Pd-MOR(150) after evacuation at 150°C was fit in r space ($2.8<k<10.8$ Å^{-1}, $1.8<r<3.4$ Å, uncorrected). The results (Table 1) indicate that after evacuation, the average cluster nuclearity has increased to ca. 4, but the Pd NN distance and Debye–Waller factor are unaltered. The Pd–O coordination number and bond distance are equivalent to those of the freshly reduced catalyst, but the Pd–O Debye–Waller factor has increased.

The EXAFS spectrum of Pd-MOR(150) after evacuation at 300°C was fit in r space ($2.8<k<10.9$ Å^{-1}, $1.0<r<3.4$ Å, uncorrected). The results (Table 1) indicate that after evacuation at 300°C the average Pd cluster nuclearity has increased to ca. 6, the Pd NN distance has contracted significantly, and the Pd–Pd shell is highly disordered. The analysis also reveals concomitant changes in Pd–O bonding: the Pd–O coordination number and disorder have increased, and the Pd–O distance has decreased to 1.97 Å.

The EXAFS spectrum of Pd-MOR after reduction at 350°C in flowing hydrogen {Pd-MOR(350)} is presented in Fig. 4(a). The high signal-to-noise ratio permits data analysis over a wide k range ($3.3<k<15$ Å^{-1}). The Pd–Pd phase-corrected Fourier transform (Fig. 4(b)) exhibits a first-shell peak near 2.7 Å; the imaginary part is nearly symmetrical within the amplitude envelope. The results of an r space fit ($1.5<r<3.5$ Å, uncorrected) evidence that reduction at 350°C yields larger Pd clusters than those found after reduction at 150°C. The Pd–Pd coordination number is consistent with cluster

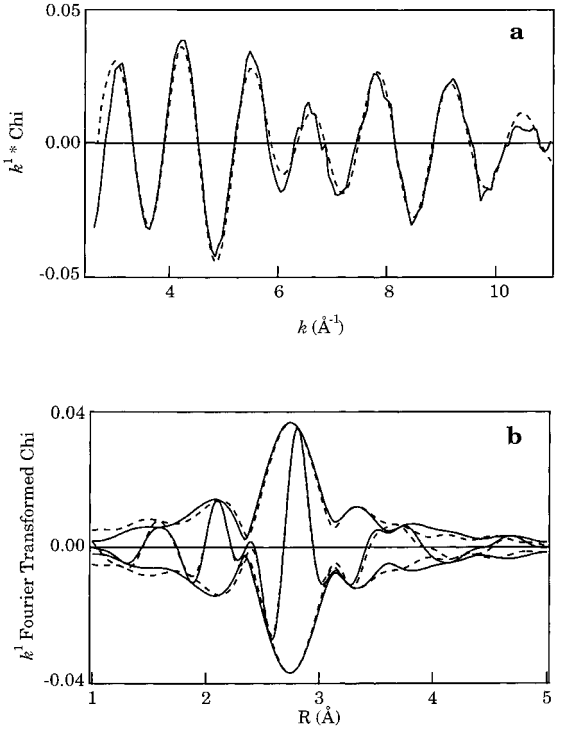

Fig. 3. Comparisons of Pd K first-shell EXAFS data (solid line) and calculated fit (dashed line) in k and r space for Pd-MOR(150): (a) k^1-weighted chi functions and (b) k^1-weighted Pd phase-corrected Fourier transforms.

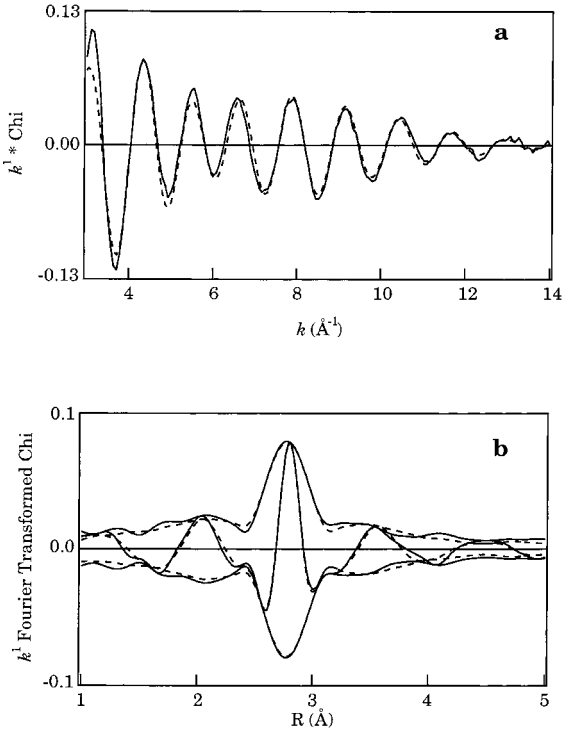

Fig. 4. Comparisons of Pd K first-shell EXAFS data (solid line) and calculated fit (dashed line) in k and r space for Pd-MOR(350): (a) k^1-weighted chi functions and (b) k^1-weighted Pd phase-corrected Fourier transforms.

nuclearity of ca. 6. Comparisons of the calculated and experimental EXAFS functions in k and r space are presented in Fig. 4. The excellent fit is consistent with the absence of significant contributions from low-Z backscatterers.

The EXAFS spectrum of Pd-MOR(350) after evacuation at 300°C is shown in Fig. 5(a). The Pd–Pd phase-corrected Fourier transform ($3.3<k<14$ Å^{-1}) (Fig. 5(b)) exhibits a first-shell peak that is larger and shifted to lower r values as compared to the spectrum of Pd-MOR(350) (Fig. 4(b)). The r space fitting results ($1.8<r<3.6$ Å, uncorrected) are given in Table 1. Evacuation at 300°C leads to increases in the Pd–Pd coordination number and Debye–Waller factor and an attendant contraction of the Pd NN distance. The Pd NN distance is shorter than that in bulk Pd consistent with the removal of chemisorbed hydrogen [10,11].

The EXAFS spectrum of Pd-MOR(350) after evacuation at 300°C and subsequent exposure to 100 Torr of CO is presented in Fig. 6(a). The data were analyzed over a wide k range ($3.1<k<14$ Å^{-1}). The Fourier transform exhibits first- and higher-shell Pd–Pd peaks (Fig. 6(b)). The results of an r space fit ($1.8<r<3.4$ Å, uncorrected) indicate the formation of large Pd clusters (Table 1). The Pd–Pd NN distance has relaxed to that of bulk Pd, and the Debye–Waller factor has decreased. Excellent fits are obtained in k and r space (Fig. 6).

The EXAFS spectrum of Pd-MOR after reduction in flowing H_2 at 450°C {Pt-MOR(450)} is indicative of large Pd clusters (Fig. 7(a)). The Pd–Pd phase-corrected Fourier transform ($2.7<k<15.0$ Å^{-1}) exhibits a larger and more symmetric first-shell peak than that observed following reduction at 350°C (Fig. 7(b)). The results of an r space fit ($1.8<r<3.5$ Å, uncorrected) are consistent with 20 Å Pd particles (Table 1). The Pd NN distance is expanded by 2.2% relative to bulk Pd suggesting the presence of interstitial hydrogen. The Debye–

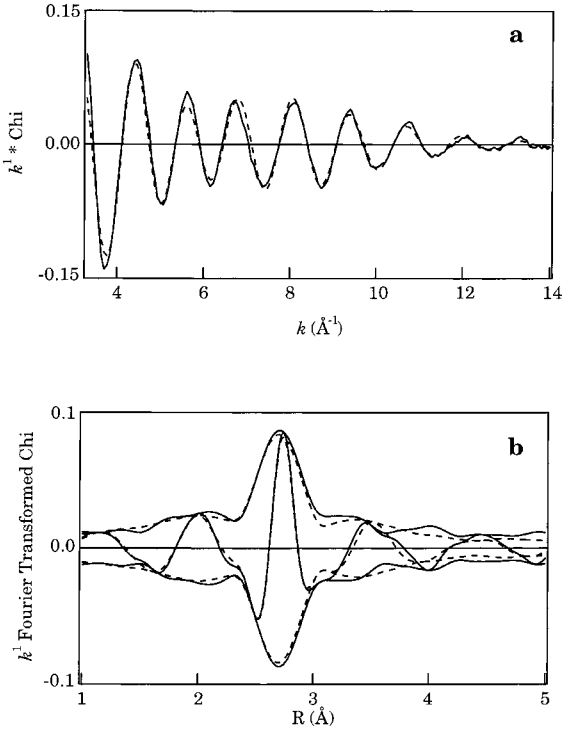

Fig. 5. Comparisons of Pd K first-shell EXAFS data (solid line) and calculated fit (dashed line) in k and r space for Pd-MOR(350) after evacuation at 300°C: (a) k^1-weighted chi functions and (b) k^1-weighted Pd phase-corrected Fourier transforms.

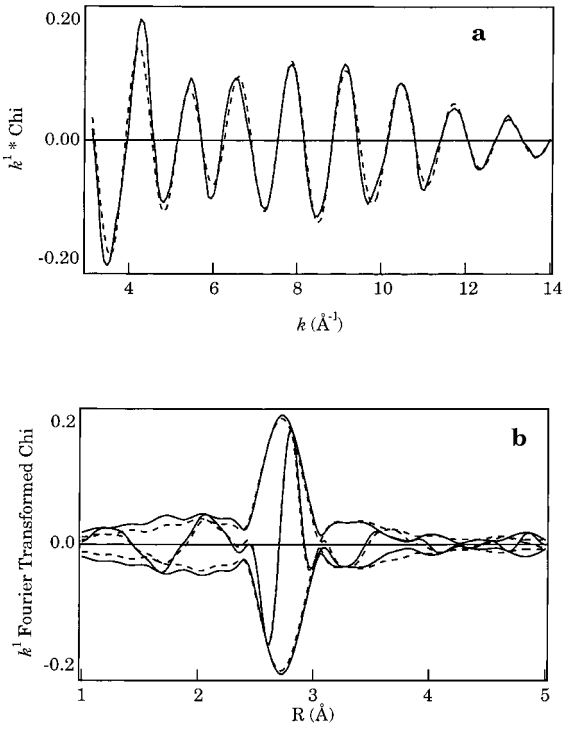

Fig. 6. Comparisons of Pd K first-shell EXAFS data (solid line) and calculated fit (dashed line) in k and r space for Pd-MOR(350) following evacuation at 300°C and subsequent exposure to 100 Torr CO: (a) k^1-weighted chi functions and (b) k^1-weighted Pd phase-corrected Fourier transforms.

Waller factor is significantly smaller than that of Pd clusters resulting from low-temperature reduction.

3.3. *FTIR spectroscopy of adsorbed* CO

The FTIR spectrum of adsorbed CO on H-MOR, resulting from calcination of NH_4-MOR at 350°C in O_2, exposure to air, and drying in flowing He at 150°C, is shown in Fig. 8. The spectrum is characteristic of species reversibly adsorbed under 100 Torr of CO at 30°C. Peaks are observed at 2170 (s) and 2140 (m) cm^{-1}. Shoulders are apparent at 2190, 2155, 2124, and 2106 cm^{-1}. No peaks remain following subsequent evacuation at 30°C.

The FTIR spectra of adsorbed CO on a calcined Pd-MOR catalyst that was exposed to air and subsequently pretreated at 150°C in flowing He in an in situ FTIR cell are shown in Fig. 9. The difference spectra were recorded in the presence of 100 Torr of CO at 30°C and after subsequent evacuation to $\sim 10^{-6}$ Torr. The difference spectrum of the catalyst under CO (Fig. 9(a)) exhibits peaks at 2218, 2190, 2165, 2144, 2122, 1984, 1955, and 1911 cm^{-1}. Following evacuation of the gaseous CO, the peaks at 2165, 2144, and 2122 cm^{-1} vanish leaving irreversibly bound species with peaks at 2218, 2190, 2133, 2115, 2095, 1984, 1955, and 1911 cm^{-1}. The infrared peaks with frequencies $\leq$2100 cm^{-1} are assigned to linear and bridging CO species on Pd^0 clusters. The remaining peaks are assigned either to CO species adsorbed on H-MOR sites or CO species on Pd^{n+} centers. The specific assignments are given in Table 2.

The FTIR difference spectra of adsorbed CO on Pd-MOR(150) are shown in Fig. 10. In comparison to Fig. 9(b), the 2190 cm^{-1} peak has disappeared, a new peak is observed at 2148 cm^{-1}, and the peaks assigned to Pd^0–CO species have increased in intensity. The

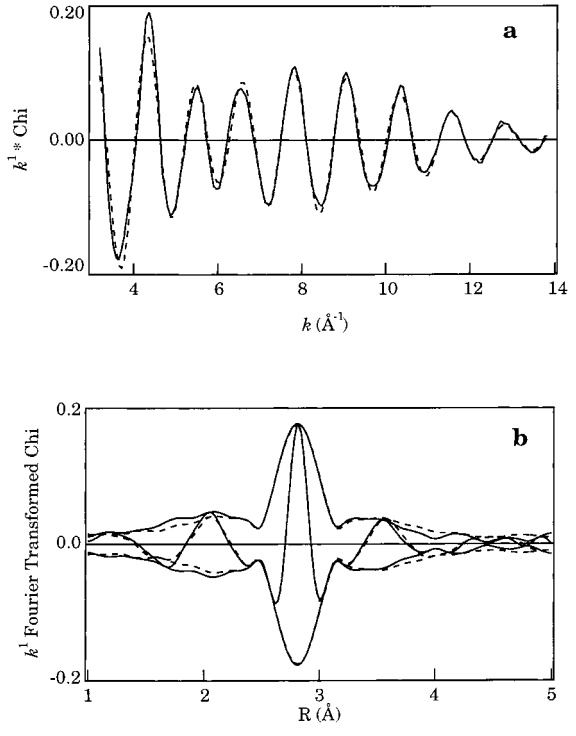

Fig. 7. Comparisons of Pd K first-shell EXAFS data (solid line) and calculated fit (dashed line) in k and r space for Pd-MOR(450): (a) k^1-weighted chi function and (b) k^1-weighted Pd phase-corrected Fourier transforms.

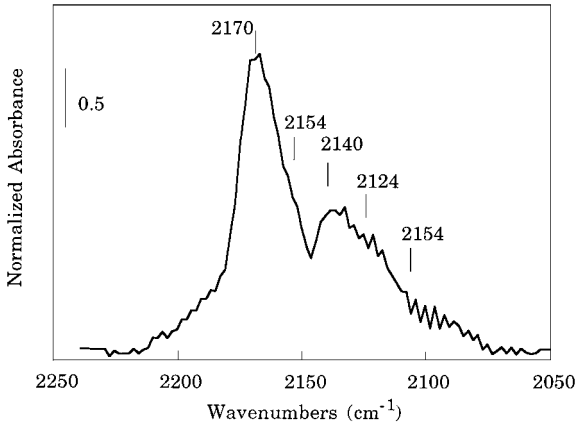

Fig. 8. Infrared difference spectrum of reversibly adsorbed CO on H-MOR.

difference spectrum (Fig. 10(a)) measured under CO contains peaks at 2175, 2158, 2142, 2124, 2089 and 1911 cm^{-1} (Table 2). The most notable changes rela-

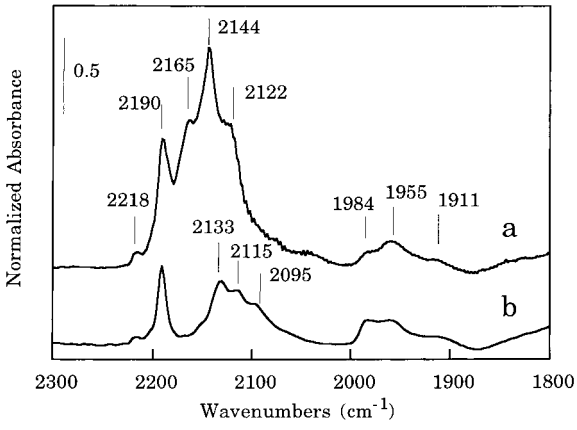

Fig. 9. Normalized infrared difference spectra of adsorbed CO on Pd-MOR: in the presence of 100 Torr of CO (a) and following subsequent evacuation (b).

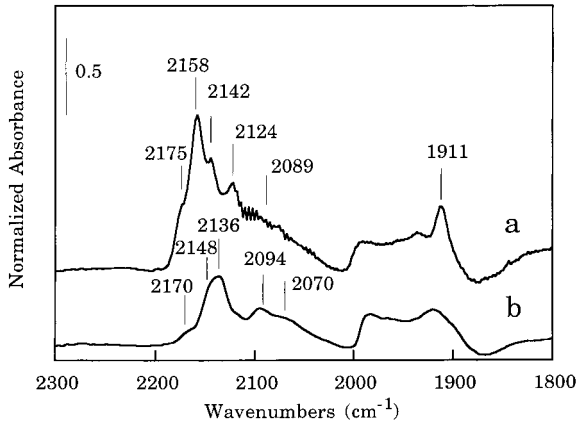

Fig. 10. Normalized infrared difference spectra of adsorbed CO on Pd-MOR(150): in the presence of 100 Torr of CO (a) and following subsequent evacuation (b).

tive to Fig. 9(a) are the elimination of the 2190 cm^{-1} band assigned to Pd^{2+} CO species, a significant intensity reduction of the 2142 cm^{-1} band, and the appearance of a well-defined peak at 1911 cm^{-1}.

The FTIR spectra of adsorbed CO on Pd-MOR(350) after pretreatment in vacuo at 300°C are shown in Fig. 11. The CO peak intensities are significantly reduced compared to those observed in the spectra of Pd-MOR and Pd-MOR(150). The peaks observed under CO at 2220 and 2200 cm^{-1} are assigned to adsorbed CO at Lewis acid sites. Weak bands assigned

Table 2
Infrared absorption frequencies of CO adsorbed on Pd-MOR catalysts[a]

Pretreatment	Pd sites				
	Pd^{2+}	Pd^{+}	$Pd^{\delta+}$	Pd^{0}(L)	Pd^{0}(B)
O_2, 350°C (ex situ)[b]	2190 (s)	2133 (s), 2115 (m)	2133 (s)	2095 (m)	1984 (m), 1955 (m), 1911 (w)
H_2, 150°C	—	2148 (s)	2136 (s)	2094 (m), 2070 (m, sh)	1984 (m), 1935 (m) 1911 (s)
H_2, 350°C; vac, 300°C	—	—	2135 (m)	2100 (m)	1985 (m), 1900 (m)

Pretreatment	Mordenite sites				
	Lewis acid	Brønsted acid	–OH	Phys. Ads. CO	Basic
O_2, 350°C (ex situ)[b]	2218 (w)	2165 (m, sh)	—	2144 (s)	2122 (m, sh)
H_2, 150°C	—	2175 (m, sh)	2158 (s)	2142 (m)	2124 (m)
H_2, 350°C; vac, 300°C	2220 (w), 2200 (w)	2168 (s)	—	2144 (m)	2125 (m,sh)

[a]Relative intensities are designated as (s) strong, (m) medium, (w) weak, (vw) very weak, and (sh) shoulder.
[b]Calcination followed by in situ treatment in He at 150°C.

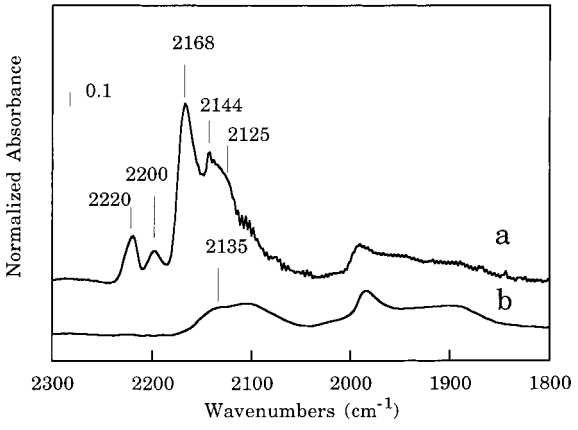

Fig. 11. Normalized infrared difference spectra of adsorbed CO on Pd-MOR(350) following evacuation at 300°C: in the presence of 100 Torr of CO (a) and following subsequent evacuation (b).

to linear and bridging CO on Pd^0 clusters are observed. After evacuation, a broad feature near 2100 cm^{-1} due to $Pd^{\delta+}$–CO and Pd^0–CO species is observed.

4. Discussion

4.1. Pd-*MOR*

Calcination of $[Pd(NH_3)_4]^{2+}$-exchanged mordenite at 350°C in O_2 results in decomposition of the amine complex and partial conversion of NH_4-MOR to H-MOR. The TPR peak temperature (Fig. 1), which exceeds the reduction temperature of bulk PdO, is consistent with reduction of Pd^{2+} complexes in mordenite [12]. The H_2 consumption (H/Pd=1.9) evidences that the heating rate during calcination was sufficiently slow to prevent significant auto-reduction via amine decomposition. The pink color observed following calcination is characteristic of an intrazeolitic Pd^{2+} oxo complex; the color change to light yellow concomitant with air exposure indicates the formation of $[Pd(H_2O)_n]^{2+}$ complexes [3]. As discussed below, the EXAFS results (Table 1), particularly the identification of a second-shell Pd–Si/Al contribution, indicate that the Pd^{2+} oxo species is located in the mordenite pores.

The EXAFS analysis of Pd-MOR evidences isolated Pd centers coordinated by ca. 4 O atoms, a structure consistent with square-planar Pd^{2+} complexes. The low Debye–Waller factor indicates that the Pd–O bonds are equivalent; therefore, it is unlikely that Pd is bound to a combination of framework oxygen, water and/or OH ligands. The presence of an outer Pd–Si/Al shell supports an assignment to framework oxygen ligands. The Pd–O distance (2.03 Å) is consistent with those reported for Pd ions coordinated to framework oxygens in X and Y zeolite [13,14]. We infer that after calcination the Pd^{2+} ions are located in the 8-ring mordenite side pockets that

line the unidirectional channels. Ca^{2+} ions exchanged in mordenite are coordinated by six oxygens in the side pockets [15], and Taarit et al. [16] identified square-planar Pd^{+} species in the side pockets using EPR.

CO adsorption was used to probe the chemistry of the Pd^{2+} species in the calcined catalyst. Recent studies have demonstrated that CO adsorbs at a variety of intracrystalline sites in H-MOR [2]. Specifically, CO reversibly adsorbs at two distinct Lewis acid sites (2218 and 2193 cm^{-1}), at a Brønsted acid site (2170 cm^{-1}), at –OH groups (2154 cm^{-1}), and at two basic sites (2124 and 2106 cm^{-1}). Physisorbed CO is observed at 2140 cm^{-1}. All of these species, except CO bonded to the stronger Lewis acid sites, are detected in the infrared spectrum of reversibly adsorbed CO on H-MOR (Fig. 8). The absence of strong Lewis sites is attributed to poisoning by adsorbed water.

Exposure of Pd-MOR to CO at 25°C results in the generation of a mixture of Pd carbonyl species, in addition to adsorbed CO at Lewis acid, Brønsted acid, and basic sites (Table 2). We assign the intense, narrow band at 2190 cm^{-1} to a Pd^{2+} monocarbonyl species, as TPR indicates that most of the Pd is initially present in the 2+ oxidation state. Pd^{2+}–CO species have been identified in Pd/Al_2O_3 and Pd/CeO_2 catalysts by ν_{CO} bands at 2160–2168 cm^{-1} [17,18], and Sheu et al. [6] assigned bands at 2176 and 2142 cm^{-1} to two different Pd^{2+} monocarbonyl species in Na-Y zeolite. We infer that the Pd^{2+}–CO species in H-MOR exhibits a higher ν_{CO} frequency due to the local intracrystalline environment. The bands at 2133 and 2115 cm^{-1} are tentatively assigned to Pd^{+} geminal dicarbonyl species on the basis of the assignment by Naccache et al. [19] of ν_{CO} bands at 2135 and 2110 cm^{-1} to Pd^{+}–$(CO)_2$ species in Y zeolite. An additional contribution to the 2133 cm^{-1} peak due to $Pd^{\delta+}$ carbonyl species is inferred (vide infra). The remaining ν_{CO} bands at $\leq$2100 cm^{-1} are assigned unambiguously to linear and bridging CO species on Pd^{0} clusters (Table 2) [17,20,21].

The chemistry resulting in generation of a mixture of Pd carbonyl species in different oxidation states by CO exposure of Pd-MOR remains to be elucidated. We suggest that the Pd^{2+} ions are reduced by CO in the presence of strongly adsorbed H_2O or –OH remaining in the mordenite pores after drying at 150°C. Redox reactions such as

$$Pd^{2+} + CO + H_2O \rightarrow Pd^{0} + CO_2 + 2H^{+}$$

$$Pd^{2+} + CO + OH \rightarrow Pd^{+} + CO_2 + H^{+}$$

are postulated.

4.2. Pd-*MOR(150)*

Reduction of the intrazeolitic Pd^{2+} oxo complex with H_2 at 150°C yields Pd clusters with an average nuclearity of ca. 3 and a Pd NN distance that is only slightly greater than in bulk Pd. A highly ordered Pd–O shell is also observed; on an average two 2.22 Å Pd–O bonds are associated with each Pd_3 cluster. The detection of a relatively short Pd–O distance might be interpreted as evidence of a mixture of segregated Pd^{n+} complexes and Pd^{0} clusters; however, we infer that the Pd–O bonds serve to anchor the Pd_3 clusters in the mordenite pores.

Both short and long metal-oxygen distances have been found to characterize the interfaces between metal clusters and metal oxide supports [11,14,22–24]. The Pd–O distance observed for Pd-MOR(150) is longer than expected for Pd^{2+}–O^{2-} ionic bonding (2.0 Å), but shorter than expected for a Pd^{0}–O^{2-} van der Waals interaction (2.8 Å). Möller et al. [14] found two Pd–O distances: 2.80 and 2.28 Å for Pd_3 clusters formed by reduction of Pd^{2+} complexes in X zeolite at 150°C. The former distance was attributed to a Pd^{0}–O^{2-} interaction; the origin of the latter distance, which is in reasonable agreement with our observations, was not discussed. The 2.22 Å Pd–O distance is suggestive of a bridging oxygen linkage similar to those found in oxide-supported metal carbonyl clusters and their molecular analogs [25]. The EXAFS spectrum of the alumina-supported triosmium carbonyl cluster $[HOs_3(CO)_{10}\{O_{support}\}]$ was found to be consistent with a surface structure in which the cluster is tethered to the support via an edge-bridging oxygen ligand [26]. The Os–$O_{support}$ coordination number and distance are 0.65 and 2.16 Å, respectively, and the Os–$O_{support}$ contribution has a low Debye–Waller factor. These EXAFS parameters are closely similar to those of Pd-MOR(150).

The infrared spectrum of strongly adsorbed CO on Pd-MOR(150) (Fig. 10(b)) is indicative of a mixture of Pd^{+}, $Pd^{\delta+}$ and Pd^{0} carbonyl species. The bands at 2148 and 2133 cm^{-1} are assigned to Pd^{+} and $Pd^{\delta+}$

carbonyl species; however, it is difficult to differentiate between Pd^{+} monocarbonyl species and linearly adsorbed CO on $Pd^{\delta+}$ clusters on the basis of their ν_{CO} frequencies. Sheu et al. [6] associated bands at 2126 and 2120 cm^{-1} with Pd^{+}–CO and $Pd^{\delta+}$–CO species, respectively, in Na-Y zeolite, and peaks near 2135 cm^{-1} are typically associated with Pd^{+}–CO species in supported Pd catalysts. Since a blue shift of ν_{CO} bands is typically observed for metal carbonyl moieties in acidic hydrogen zeolites [27], we infer that the bands at 2148 and 2133 cm^{-1} are due to Pd^{+}–CO and polynuclear $Pd^{\delta+}$ carbonyl species, respectively. We suggest that the Pd^{+}–CO moieties are produced by CO-induced oxidative fragmentation of the small Pd clusters initially present after 150°C reduction. The CO-induced fragmentation of supported clusters is well established for Rh/γ-Al_2O_3 catalysts [24,25] and has been recently reported for Pt clusters in L zeolite [28]. The peaks assigned to Pd^{0} sites include two linear CO species, one doubly bridging CO species, and two triply bridging CO species (Table 2). We speculate that the sharp peak at 1911 cm^{-1} may arise from triply bridging carbonyl moieties on triangular faces of Pd_3 clusters. The weak band at 2170 cm^{-1} is tentatively assigned to adsorbed CO at strong Brønsted acid sites.

The Pd-MOR(150) EXAFS results evidence a slightly expanded Pd NN distance. The Pd NN distance in bare Pd clusters is expected to be shorter than in bulk Pd metal; however, an expanded Pd NN distance has been observed for silica-supported Pd_6 clusters under a H_2 atmosphere due to Pd hydride formation [10,29]. Hydride decomposition was observed upon heating the silica-supported Pd_6 clusters at 150°C in vacuo, as evidenced by contraction of the Pd–Pd distance. In contrast, EXAFS analysis following evacuation of Pd-MOR(150) at 150°C does not show a contraction of the Pd NN distance. This indicates that the intrazeolitic Pd_3 clusters do not form interstitial hydride species; evidently, the Pd_3 clusters are too small to provide the required sites. The slightly expanded NN distance in the intrazeolitic Pd_3 clusters may be a consequence of Pd–O bonding. The average Pd–O coordination number and distance are unchanged after evacuation at 150°C, but the disorder has increased slightly. Since the Pd–Pd coordination number has increased, there are on an average 2–3 Pd–O bonds per Pd_4 cluster.

Heating a freshly reduced Pd-MOR(150) sample at 300°C in vacuo results in cluster aggregation and concomitant contraction of the Pd NN distance (2.67 Å). A large increase in the disorder of the Pd–Pd shell is also observed. The EXAFS results are indicative of bare intrazeolitic Pd clusters, resulting from removal of chemisorbed H_2. The increased disorder reflects a broader distribution of Pd–Pd bond distances. The extent of aggregation suggests that the clusters are no longer anchored within the pores after evacuation at 300°C. Consistent with this hypothesis, a decrease in the Pd–O distance and a small increase in the Pd–O coordination number are observed. The resultant bond distance is indicative of a Pd^{2+}–O^{2-} ionic bonding. We infer that during evacuation at 300°C the Pd centers that anchor the original Pd clusters in the mordenite pores are oxidized via electrophilic attack of zeolite protons. The resultant Pd^{2+} species are bonded to framework oxygens and do not interact strongly with the Pd^{0} clusters.

4.3. Pd-*MOR(350)*

Reduction of Pd-MOR with H_2 at 350°C results in Pd clusters with an average nuclearity of 6 and a Pd NN distance slightly larger than in bulk Pd. The EXAFS results are consistent with Pd_6 hydride clusters hosted in the mordenite pores. The critical dimension of an octahedral Pd_6 cluster (6.6 Å) is small enough to allow it to fit within the 6.7×7.0 Å elliptical channels. The Pd clusters exhibit an NN distance and Debye–Waller factor closely similar to those found for Pd-MOR(150); however, there is no evidence of Pd–O bonding.

Heating Pd-MOR(350) at 300°C in vacuo results in cluster aggregation with concomitant contraction of the Pd NN distance and increase in the Debye–Waller factor. The shorter Pd NN distance and larger Debye–Waller factor are characteristic of bare Pd clusters. The NN distance is longer than in the bare Pd_6 clusters formed by evacuation of Pd-MOR(150) at 300°C, consistent with the larger cluster size. The average cluster size (∼10 Å) dictates that some of the clusters either reside on external mordenite surfaces or locally disrupt the mordenite pore structure [30]. The absence of a Pd–O contribution indicates that evacuation at 300°C does not re-oxidize the Pd.

Subsequent CO exposure of Pd-MOR(350) results in further cluster aggregation with attendant increase in the Pd NN distance and decrease in the Debye–Waller factor. The size of the resultant clusters (∼20 Å) is significantly larger than the mordenite pore dimensions, indicating either Pd migration to external mordenite surfaces or local framework disruption. Zhang et al. [11] observed similar CO-induced aggregation of Pd clusters in NaY zeolite and postulated that CO adsorption weakens the interaction of the clusters with the pore walls, forming mobile Pd carbonyl complexes that coalesce to form larger clusters. The changes in Pd–Pd bonding following CO exposure are due to two factors: increased cluster size and coordinative saturation of surface Pd atoms by CO. We find that in general the Debye–Waller factor is lower for CO-covered Pd clusters than for bare Pd clusters of a similar size. The reduction in disorder may have static and dynamical contributions.

The weak Pd carbonyl ν_{CO} bands (Fig. 11) observed following exposure of Pd-MOR(350) to CO at 30°C are consistent with Pd cluster aggregation. In addition to bands assigned to linear and bridging CO on Pd^0 clusters, a broad shoulder at 2135 cm^{-1} is observed which indicates the presence of polynuclear $Pd^{\delta+}$–CO species. Under 100 Torr of CO, ν_{CO} bands that are assigned to adsorbed CO at Lewis and Brønsted acid sites are observed; however, the overall intensity of bands assigned to adsorbed CO at intracrystalline mordenite sites is diminished greatly in comparison to the spectra of Figs. 9 and 10. This suggests that the large Pd clusters formed by CO-induced aggregation may block the mordenite pores.

4.4. Pd-*MOR(450)*

Reduction of Pd-MOR in H_2 at 450°C yields large Pd clusters of a similar size (∼20 Å) to those found after CO exposure of Pd-MOR(350); however, the expanded Pd NN distance is characteristic of Pd hydride formation. The 2.2% "lattice expansion" is greater than observed for the Pd_6 clusters of Pd-MOR(350) and closer to that observed in bulk Pd hydride (3.5%), consistent with the larger cluster size. The lower Debye–Waller factor evidences that the larger Pd hydride clusters have a more ordered structure, as expected.

5. Conclusions

- Calcination of $[Pd(NH_3)_4]^{2+}$-exchanged mordenite at 350°C in O_2 results in decomposition of the amine complex and formation of Pd^{2+} oxo species. The Pd-MOR EXAFS results are consistent with square-planar Pd^{2+} complexes located in the 8-ring mordenite side pockets.
- Reduction of Pd-MOR in H_2 at 150°C yields Pd clusters with an average nuclearity of 3. On an average two 2.22 Å Pd–O bonds are associated with each Pd_3 cluster, and we infer that this interaction serves to anchor the clusters within the pores. The FTIR spectrum of irreversibly adsorbed CO on Pd-MOR(150) is indicative of a mixture of Pd^+, $Pd^{\delta+}$, and Pd^0 carbonyl species. The intrazeolitic Pd_3 clusters apparently lack the required interstitial sites for Pd hydride formation. Heating in vacuo at 300°C results in oxidation of interfacial $Pd^{\delta+}$ centers to Pd^{2+} with concomitant formation of bare Pd_4 clusters.
- Reduction of Pd-MOR at 350°C in H_2 produces intrazeolitic Pd_6 clusters that exhibit only a weak interaction with the mordenite pores as evidenced by their facile aggregation in the presence of CO at 30°C.
- Reduction at 450°C yields large 20 Å Pd clusters that we infer are located on external mordenite surfaces or locally disrupt the intracrystalline structure.

Acknowledgements

The authors gratefully acknowledge the contributions of Prof. D.E. Sayers and the staff of beamline X-11 at the National Synchrotron Light Source. This research was supported by an NSF Presidential Young Investigator Award (CTS-8958350). SNR acknowledges financial assistance in the form of a Ph.D. fellowship from Hoechst-Celanese Corporation.

References

[1] W.M.H. Sachtler, Z. Zhang, Adv. Catal. 39 (1993) 129.
[2] V. Gruver, J.J. Fripiat, J. Phys. Chem. 98 (1994) 8549.
[3] B.T. Carvill, B.A. Lerner, Z. Zhang, W.M.H. Sachler, J. Catal. 143 (1993) 314.

[4] E.S. Shpiro, G.N. Baeva, A.S. Sass, V.A. Shvets, A.B. Fasman, V.B. Kazanskii, K.M. Minachev, Kinet. Catal. 28 (1988) 1236.
[5] B.C. Gates, D.C. Koningsberger, CHEMTECH 22 (1992) 300.
[6] L.L. Sheu, H. Knozinger, W.M.H. Sachtler, J. Mol. Catal. 57 (1989) 61.
[7] D.E. Sayers, B.A. Bunker, in: D.C. Koningsberger, R. Prins (Eds.), X-Ray Absorption: Principles, Applications, Techniques of EXAFS, SEXAFS, and XANES, Wiley, New York, 1988, p. 211.
[8] M. Vaarkamp, J.C. Linders, D.C. Koningsberger, Physica B 208, 209 (1995) 159.
[9] J. Mustre de Leon, J.J. Rehr, S.I. Zabinsky, R.C. Albers, Phys. Rev. B 44 (1991) 4146.
[10] S.N. Reifsnyder, H.H. Lamb, Catal. Lett. 40 (1996) 155.
[11] Z. Zhang, H. Chen, W.M.H. Sachtler, J. Chem. Soc., Faraday Trans. 87 (1991) 1413.
[12] S.T. Homeyer, W.M.H. Sachtler, J. Catal. 118 (1989) 266.
[13] G. Bergeret, P. Gallezot, B. Imelik, J. Phys. Chem. 85 (1981) 411.
[14] K. Möller, D.C. Koningsberger, T. Bein, J. Phys. Chem. 93 (1989) 6116.
[15] W.J. Mortier, J.J. Pluth, J.V. Smith, Mater. Res. Bull. 11 (1976) 15.
[16] B. Taarit, J.C. Vedrine, J.F. Dutel, C. Naccache, J. Mag. Resonance 31 (1978) 251.
[17] A. Palazov, C.C. Chang, R.J. Kokes, J. Catal. 36 (1975) 338.
[18] L.M. Kustov, W.M.H. Sachtler, J. Mol. Catal. 71 (1992) 233.
[19] C. Naccache, M. Primet, M.V. Mathieu, Adv. Chem. Ser. 122 (1973) 266.
[20] J. Szanyi, W.K. Kuhn, D.W. Goodman, J. Vac. Sci. Tech. 11 (1993) 1969.
[21] P. Gelin, A.R. Siedle, J.J.T. Yates, J. Phys. Chem. 88 (1984) 2978.
[22] J.-R. Chang, D.C. Koningsberger, B.C. Gates, J. Am. Chem. Soc. 114 (1992) 6460.
[23] P. Lagarde, T. Murata, B. Vlaic, E. Freund, H. Dexpert, J.P. Bournonville, J. Catal. 84 (1983) 333.
[24] H.F.J. van't Blik, J.B.A.D. van Zon, T. Huizinga, J.C. Vis, D.C. Koningsberger, R. Prins, J. Am. Chem. Soc. 107 (1985) 3139.
[25] H.H. Lamb, B.C. Gates, H. Knözinger, Angew. Chem. Int. Ed. Engl. 27 (1988) 1127.
[26] F.B.M. Duivenvoorden, D.C. Koningsberger, Y.S. Uh, B.C. Gates, J. Am. Chem. Soc. 108 (1986) 6254.
[27] M.M. Otten, M.J. Clayton, H.H. Lamb, J. Catal. 149 (1994) 211.
[28] B.L. Mojet, D.C. Koningsberger, Catal. Lett. 39 (1996) 191.
[29] J.A. McCaulley, J. Phys. Chem. 97 (1993) 10372.
[30] F.W.H. Kampers, C.W.R. Engelen, J.H.C.v. Hooff, D.C. Koningsberger, J. Phys. Chem. 94 (1990) 8574.